ACS APPLIED MATERIALS & INTERFACES
Research Article
www.acsami.org

Double-Patterned Sidewall Directed Self-Assembly and Pattern Transfer of Sub-10 nm PTMSS-*b*-PMOST

Julia Cushen,*[,†] Lei Wan,[†] Gregory Blachut,[‡] Michael J. Maher,[§] Thomas R. Albrecht,[†] Christopher J. Ellison,[‡] C. Grant Willson,[‡,§] and Ricardo Ruiz[†]

[†]HGST, a Western Digital Company, 3403 Yerba Buena Rd., San Jose, California 95135, United States

[‡]The University of Texas at Austin, McKetta Department of Chemical Engineering, 200 E Dean Keeton St. Stop C0400, Austin, Texas 78712, United States

[§]The University of Texas at Austin, Department of Chemistry, 105 E. 24th St. Stop A5300, Austin, Texas 78712, United States

Supporting Information

ABSTRACT: The directed self-assembly (DSA) of two sub-20 nm pitch silicon-containing block copolymers (BCPs) was accomplished using a double-patterned sidewall scheme in which each lithographic prepatterned feature produced two regions for pattern registration. In doing so, the critical dimension of the lithographic prepatterns was relaxed by a factor of 2 compared to previously reported schemes for DSA. The key to enabling the double-patterned sidewall scheme is the exploitation of the oxidized sidewalls of cross-linked polystyrene formed during the pattern transfer of the resist via reactive ion etching. This results in shallow trenches with two guiding interfaces per prepatterned feature. Electron loss spectroscopy was used to study and confirm the guiding mechanism of the double-patterned sidewalls, and pattern transfer of the BCPs into a silicon substrate was achieved using reactive ion etching. The line edge roughness, width roughness, and placement error are near the target required for bit-patterned media applications, and the technique is also compatible with the needs of the semiconductor industry for high-volume manufacturing.

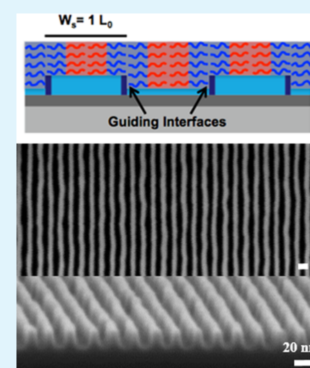

KEYWORDS: *block copolymer, directed self-assembly, top coat, silicon-containing, sidewall-guiding, chemical contrast patterns, density multiplication*

INTRODUCTION

Block copolymer (BCP) lithography has increasingly gained momentum as a solution for creating the small features required for high areal density patterning in the storage and semiconductor industries.[1−3] Line/space patterns formed by BCPs are particularly attractive to define fin elements for Fin FETs[4] or to define rectangular arrays of islands for magnetic recording bit patterned media (BPM).[5] While BCPs do not form rectangular lattices naturally, it has been shown that rectangular arrays can be formed by the orthogonal intersection of two independent line/space templates.[6] The number of available symmetric BCPs suitable for sub-10 nm lithography is limited, and yet, the single-digit nm regime is decisive to enable BPM technology above 1.2 Tdot/in^2 and to extend semiconductor lithography beyond the 11 nm node. Both applications demand a full pitch below 20 nm (half pitch below 10 nm). Symmetric poly(styrene-*b*-methyl methacrylate), PS-*b*-PMMA, is the most mature and the most studied lamellar BCP but is limited by a relatively weak interaction parameter, χ, that restricts the smallest lithographic dimensions it can form to around 10−11 nm (20−22 nm full pitch). Although phase separation at smaller dimensions has been reported from 19 to 17.5 nm pitch, no pattern transfer of PS−PMMA has yet been demonstrated in this regime,[7−9] so any directed self-assembly (DSA) solution below 20 nm pitch will most likely need a BCP with a χ value higher than that of PS-*b*-PMMA.

Silicon-containing BCPs are particularly promising to extend BCP lithography beyond PS-*b*-PMMA. They commonly exhibit a χ value that is high enough to enable phase separation below 20 nm full pitch.[10−12] Additionally, the silicon in the Si-containing block can be oxidized to form a densified SiO structure that provides etch contrast for both removal of the organic block and for pattern transfer into the substrate. Producing perpendicularly oriented lamellae to form line/space patterns with Si-containing BCPs had been, until recently, an elusive goal because the lower surface energy of the Si-containing block drives the formation of a preferential wetting layer at the free surface, inducing orientation of the lamellae parallel to the free interface. In recent work, this challenge was addressed specifically for block copolymers based on poly(4-trimethylsilylstyrene), PTMSS, by designing a polarity-switching top coat that tailors the interfacial energy at the top of the film to induce perpendicular orientation of the domains.[13−16]

Conventional DSA relies on chemical patterns to guide the self-assembly of BCPs.[17−20] Scaling DSA below 20 nm pitch

Received: March 23, 2015
Accepted: May 25, 2015
Published: May 25, 2015

© 2015 American Chemical Society

DOI: 10.1021/acsami.5b02481
ACS Appl. Mater. Interfaces 2015, 7, 13476−13483

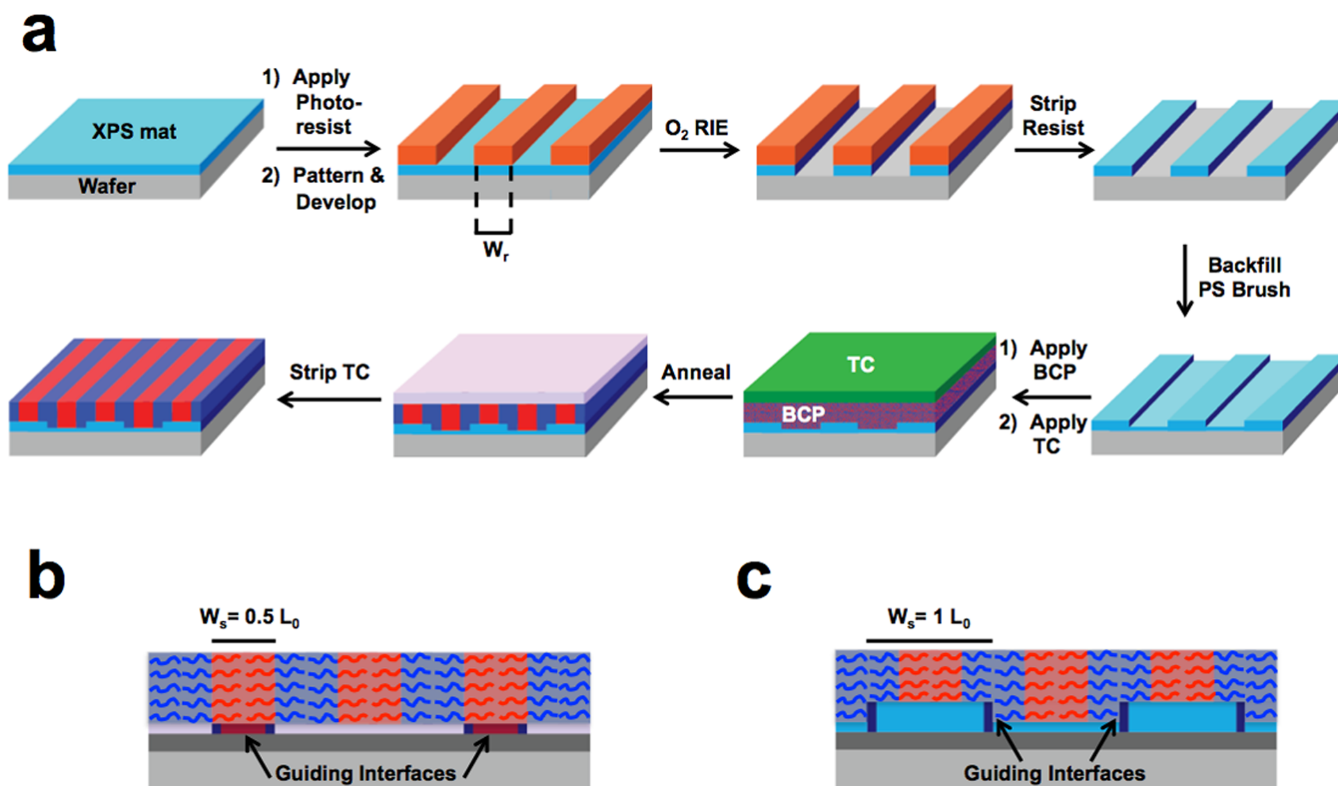

Figure 1. (a) Process flow for creating doubled patterned oxidized sidewalls on PS mat that serve as guiding interfaces and subsequent BCP directed assembly, (b) the orientation of individual polymer chains in conventional chemical guiding using the top of the mat as the guiding interface where $W_s = {}^1/_2\ L_o$, and (c) the orientation of individual polymer chains in double-patterned sidewall guiding DSA where the oxidized sidewalls are the guiding interfaces and where $W_s = L_o$.

involves much more than just a higher χ BCP; the fabrication of the chemical contrast pattern presents resolution challenges. Currently the trim-etch flow is being integrated for high volume manufacturing.[21] In this process, a cross-linked polymer mat that is preferential for one domain of the BCP is coated and patterned with e-beam and photoresist.[22,23] An array of line/space patterns is exposed on the resist and developed. The pitch in the resist pattern can be sparse as long as it is commensurate to that of the block copolymer, but the resist width, w_r, must be tuned to match the width of the one block copolymer domain, $w_r = {}^1/_2\ L_o$ (Figure 1a). This resist pattern is then used as a mask to etch portions of the cross-linked polymer mat, generating an array of mat line/space patterns that matches the dimensions of the resist pattern. The etched spaces between mat lines in the background region are backfilled with random copolymer brushes with average compositions engineered to minimize the interfacial energy with the overlying block copolymer that contacts these regions. The top surfaces of the mat lines serve as guiding interfaces that align the assembled block copolymer. As critical dimensions shrink below 10 nm and higher χ solutions are required for scaling, DSA faces two important challenges: (1) it is increasingly difficult for the faster positive tone resists to achieve resolutions that match ${}^1/_2\ L_o$, and (2) brush chemistries must be independently developed and tuned for each BCP for each density multiplication scheme.[24−26]

We report a method that allows relaxation of the resolution requirement of w_r in the initial lithographic step by using the oxidized sidewalls of the PS mat as the guiding interface for DSA. Utilizing this double patterning technique to generate the chemical contrast patterns has advantages over the conventional methods because it multiplies the density of guiding interfaces by a factor of 2, therefore relaxing the resolution requirement of the patterned resist to $w_r = L_o$. We use a generic PS mat and PS−OH brush because its wetting characteristics are intermediate between the two blocks, which has been determined using previously reported methodology.[14,27] A shallow trench between the mat and backfilling brush also assists in guiding the BCP domains, thus combining graphoepitaxy with chemical epitaxy without the concomitant loss of usable area common to graphoepitaxy techniques. The effectiveness of this sidewall double patterning DSA was exemplified by carrying out the first demonstration of pattern transfer into a Si substrate using a poly(trimethylsilylstyrene-*block*-*p*-methoxystyrene) (PTMSS-*b*-PMOST) block copolymer with a full pitch under 20 nm. Two lithographically relevant dimensions are demonstrated: 19.9 and 17.4 nm full pitch. Supporting evidence for the proposed guiding mechanism is provided by an elemental mapping from electron energy loss spectroscopy (EELS). Line roughness and defect densities are discussed in the context of BPM requirements.

■ EXPERIMENTAL SECTION

We investigated DSA with two lamellae-forming PTMSS-*b*-PMOST BCPs with a pitch of 19.9 and 17.4 nm. A random copolymer mat and a top coat polymer were used to promote perpendicular orientation as described in previous work.[15,28] The random copolymer mat was only used for undirected assembly and synthesis protocols for the block copolymers and mat were previously reported.[15] Details related to the material characterization are reported in the Supporting Information. The fingerprint pattern pitch of the perpendicularly oriented BCPs on neutral cross-linked surface treatments were measured after thermal annealing by an image analysis protocol described elsewhere[29] and are denoted hereafter by a numerical subscript corresponding to the pitch.

DOI: 10.1021/acsami.5b02481
ACS Appl. Mater. Interfaces 2015, 7, 13476−13483

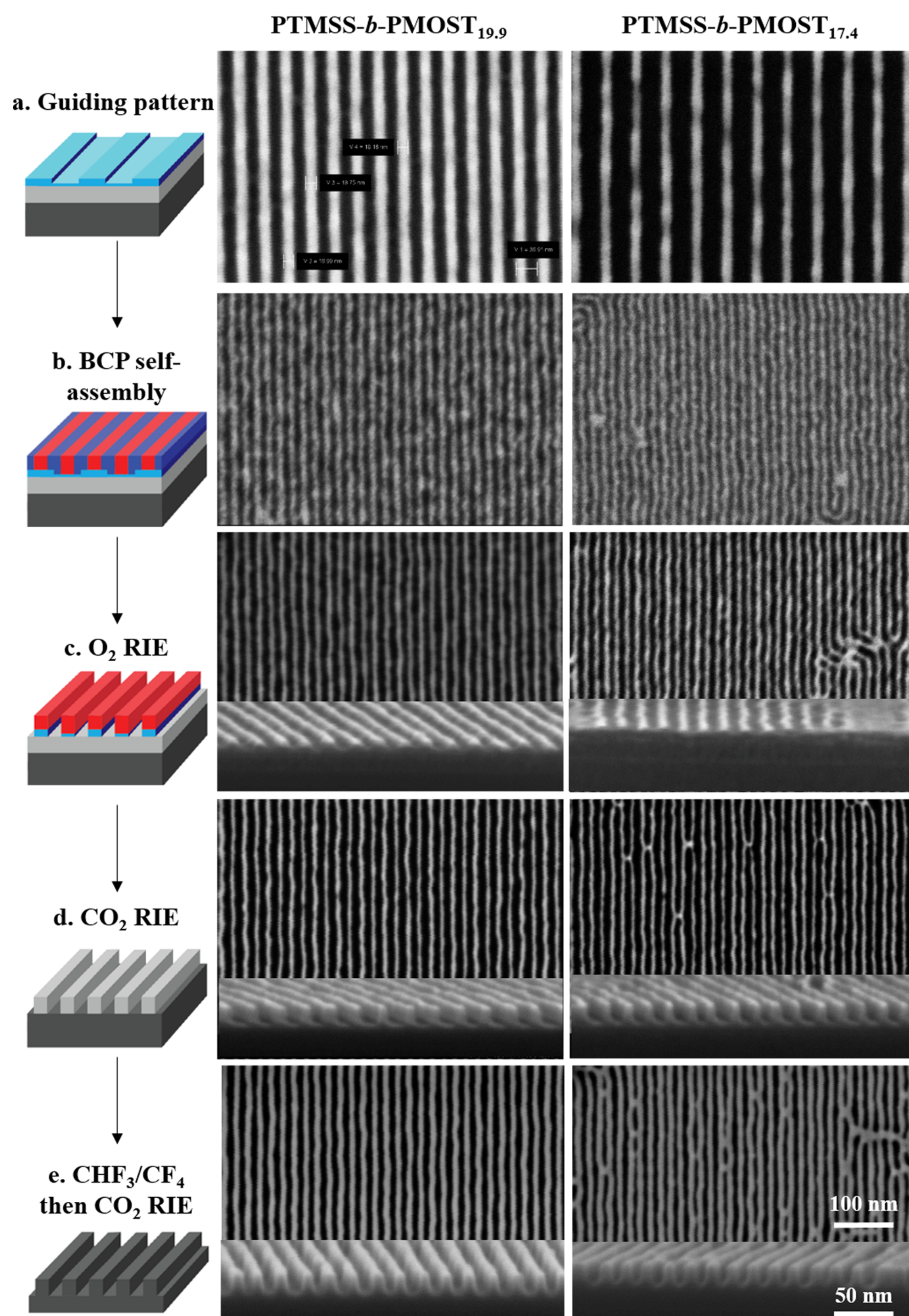

Figure 2. Cartoon of the pattern transfer process with top-down and cross-section images of PTMSS-*b*-PMOST$_{19.9}$ and PTMSS-*b*-PMOST$_{17.5}$ at each etch step. (a) Chemical contrast pattern on DLC (b) BCP film stack after annealing and top coat removal (brief O_2 etch was performed for SEM contrast), (c) after O_2 RIE to remove PMOST and oxidize the PTMSS (d) after subsequent CO_2 RIE to transfer into DLC (e) after CHF_3/CF_4 RIE into Si substrate and carbon removal with CO_2 RIE.

For DSA, a cross-linkable PS-mat[23] and a 1.2 kDa PS−OH brush (Polymer Source) were used as surface modification materials.

Double-patterned, oxidized polystyrene mat sidewall patterns for DSA were obtained following the protocol shown in Figure 1a. A Si substrate coated with 17 nm of a diamond-like carbon (DLC) film by ion beam deposition (not shown) was coated with 8 nm of PS mat. E-beam resist (ZEP) was deposited on top of the mat and exposed using a rotary e-beam tool. The exposed patterns (orange features in Figure 1a) consisted of line/space arrays with a pitch, L_s, of 2 L_o or 3 L_o and $w_r = L_o$, where w_r is the width of the remaining resist lines and L_o represents the full pitch of the block copolymer to be used. Following a similar protocol to that used in conventional chemoepitaxy, the exposed portions of the mat film were subjected to O_2 reactive ion etching (RIE) to form PS mat stripes. The sidewalls of the PS mat were also oxidized during the O_2 RIE step[30] altering their chemistry to form two oxidized sidewalls for every PS line (darker mat sidewalls in Figure 1a). Similar to the spacer lines in self-aligned double patterning,[31,32] this surface modification of the sidewalls may be viewed as a double patterning technique.[33]

In conventional chemical contrast patterns where $W_s = {}^1/_2\ L_o$,[23] the space between the mat lines is backfilled with a random copolymer brush

DOI: 10.1021/acsami.5b02481
ACS Appl. Mater. Interfaces 2015, 7, 13476−13483

with a composition that minimizes the average interfacial energy with the portion of the block copolymer that assembles on top. As a result, the block that has a stronger affinity for the polymer mat assembles on top and directs the assembly of the film (Figure 1b). This process has proven to be very robust thanks to the engineering of the boundary conditions that match the free energy minimum to the lithographically desired morphology. However, as dimensions scale down below 10 nm, it is increasingly challenging to trim the width of the prepatterns down to the desired W_s. The resolution limitations of the guiding line width can be overcome by patterning guiding lines that are multiples of $^1/_2$ L_o, and the pitch can be multiplied by increasing the space between the lines by some integer multiple of L_o.[34] However, the defectivity of these patterns typically increases with fewer and wider guiding lines.

DSA using double-patterned sidewall guiding lines is believed to occur by a chain configuration and interaction mechanism that is shown in Figure 1c. We propose that oxidation of the sidewalls takes place during the etching of the PS mat,[30] which alters the chemistry and modifies the surface energy of the sidewalls. The backfilling brush was chosen to be purposely short (1.2 kDa) to produce a shallow trench (∼5 nm) such that a portion of the mat sidewalls is still exposed after brush backfilling. The oxidized mat sidewall is strongly wet by one of the polymer blocks. Hence, the assembly is directed by preferential wetting of the oxidized sidewall inside the shallow trench. On the basis of the expected wetting behavior of PTMSS and PMOST with oxidized PS and results from cross-sectional transmission electron microscopy, TEM, detailed later in this study, we believe PTMSS is the "red" block and PMOST is the "blue" block in Figure 1c. The trench width was chosen to be commensurate with the block copolymer pitch so that the stripes align parallel to the trench walls. While the shallow trench plays an important role directing the assembly by providing confinement, it is not enough to induce the selective registration between the PMOST domains and the oxidized sidewalls. It has been reported in the past, both theoretically and experimentally, that when there is only topography, the molecules align with their long axes parallel to the topographic steps, causing the domain stripes to be perpendicular to the trenches due to restrictions in chain packing.[35−38] We observed this orientation (Figure S3, Supporting Information) with 80 nm pitch guiding structures with a 40 nm width. Without enough guiding interfaces to induce parallel orientation, the domains oriented perpendicular to the guiding lines due to the shallow topography.

The double-patterned sidewall guiding strategy has some elements of both graphoepitaxy and chemoepitaxy[39] but does not sacrifice usable area because the BCP self-assembles both inside and outside the trenches. Previous demonstrations of graphoepitaxy with lamellar block copolymers restrict the assembly only within the guiding trench rendering the area between trenches unusable.[39,40] Figure 1b,c demonstrates the differences in guiding interface formation and polymer chain configurations between conventional chemical contrast pattern guided and double-patterned sidewall guided DSA. It should be noted that these figures are likely oversimplified. In conventional DSA, there may be some shallow topography that is not shown in Figure 1b, and the sidewalls of the mat lines may not be completely vertical in either strategy. We also note that sidewall oxidation also occurs in conventional chemoepitaxy; however, the use of longer backfilling brushes that cover most of the sidewalls are likely to mask or diminish the effect of the sidewall chemistry.

The wetting behavior of the PS mat, oxidized PS mat, PMOST, and PTMSS homopolymer films were investigated by water contact angle measurements.[41,42] The PS mat was prepared in a manner identical to that in the chemical contrast patterns except as a full film without e-beam patterning. The oxidized PS mat was prepared by exposing a full film PS mat to the same O_2 RIE used in creation of the chemical contrast patterns to simulate the oxidation of the sidewall on the surface. A dramatic decrease in the water contact angle was observed for oxidized PS mat (28°) compared to PS mat (86°). Topography in the guiding pattern was characterized by AFM, which revealed about a 5 nm height difference between the backfill brush and mat guiding line. These data, in addition to the water contact angle details, are reported in the Supporting Information.

One consequence of the double-patterned sidewall guiding DSA is that unlike conventional chemical contrast guiding, the combined surface energy of the substrate (i.e., with weighted contributions from the guiding structures and backfill brush chemistries) is not necessarily intermediate to that of the two BCP domains. Conventional chemical contrast patterns made from polymer mats and brushes have an average surface energy of the substrate that exhibits neutral wetting. By contrast, in double-patterned sidewall guiding DSA, the wetting behavior of the sidewall pins the assembly inside the trench; the chemistry of the surfaces in the plane of the substrate (the top of the mat and backfilling brush) are not tuned separately. As a consequence, there may be an imbalance in the wetting properties that is compensated by the confinement in the trench and by entropic restrictions set by the film thickness. Vertical orientation of the BCP domains inside the trench is induced by the topographic feature and by the preferential sidewall wetting.[39] On top of the mat line, the perpendicular orientation is sustained over a narrow window of thickness values for which the vertical orientation is more energetically favored.[43,44] Outside of that narrow thickness process window (1−2 nm), patches of parallel orientation were observed (image provided in Supporting Information), indicating that the overall substrate interface is likely off-neutral. In-plane registration of the domains on top of the mat lines is induced by interaction with the oxidized sidewalls. Note that the number of guiding features in this process flow is twice the number of the lithographically defined lines. In what follows, we keep the standard nomenclature for the density multiplication factor as the ratio between the pitch of the mat stripes to the pitch of the block copolymer lines (L_s/L_o). Thus, for the example of Figure 2c, where $L_s = 2L_o$ we refer to a density multiplication of 2× even when there is one oxidized PS sidewall per every PMOST domain. For a 3× density multiplication, there are two oxidized PS sidewalls per every three PMOST domains, and so on.

PTMSS-*b*-PMOST$_{19.9}$ was aligned by double-patterned sidewall DSA at 2× density multiplication with L_s = 40 nm and W_s = 20 nm. Due to resolution limitations by the e-beam resist, PTMSS-*b*-PMOST$_{17.4}$ had to be aligned at 3× density multiplication with L_s = 52 nm and W_s = 17 nm (Figure 2a). Once the domains of these BCPs were aligned by thermal annealing with a top coat (Figure 2b), the line pattern was transferred into the underlying silicon substrate through a series of RIE steps. Because the silicon in the PTMSS oxidizes during the first RIE step and silicon oxide is not a good etch mask for pattern transfer into a silicon substrate with a fluorine etch chemistry, the only etch chemistry available at the time of these experiments, diamond-like carbon (DLC) was used as a transfer layer between the oxidized PTMSS and silicon substrate. After the first oxidation and PMOST removal etch step was performed (Figure 2c), a subsequent CO_2 etch was used to transfer the silicon oxide pattern into DLC (Figure 2d). The patterned DLC was used as an etch mask in a CHF_3/CF_4 etch step to transfer the pattern into silicon. An additional CO_2 etch step was performed to remove any residual DLC on top of the silicon features (Figure 2e).

The guided PTMSS-*b*-PMOST$_{19.9}$ and PTMSS-*b*-PMOST$_{17.4}$ patterns were transferred into the substrate with good sidewall quality, indicating that oxidized PTMSS creates a sufficient etch mask for transfer into DLC and subsequent transfer into silicon. However, as observed in Figure 2, the defect rate was significantly larger for PTMSS-*b*-PMOST$_{17.4}$ indicating the need for further optimization. Defect sources and solutions for PTMSS-*b*-PMOST$_{19.9}$ will be discussed later in this manuscript. We also measured line roughness using an image analysis described elsewhere[45] from square SEM images 1.8 μm long with a pixel size of 0.9 nm. The line roughness values for PTMSS-*b*-PMOST$_{19.9}$ after oxidizing PTMSS and removing the PMOST, were $3\sigma_p$ = 2.3 nm, $3\sigma_w$ = 2.3 nm, $3\sigma_e$ = 2.6 nm for placement, width, and edge roughness, respectively (placement roughness refers to the roughness of the centroid line). The corresponding values after pattern transfer into the Si substrate were $3\sigma_p$ = 2.6 nm, $3\sigma_w$ = 2.3 nm, $3\sigma_e$ = 2.9 nm. A minimal increase in placement and edge roughness occurred after transfer into Si. The width roughness remained unchanged suggesting that width roughness is primarily limited by the PTMSS and its oxidation process. The 1-σ values represent ∼4% of the pitch for the placement roughness and ∼8% of the line width for the width roughness. For BPM applications, both of these numbers are targeted to be below

DOI: 10.1021/acsami.5b02481
ACS Appl. Mater. Interfaces 2015, 7, 13476−13483

5%.[5,46] The placement roughness is already below target, and the width roughness is promising considering that this is the first demonstration of DSA and pattern transfer using a Si-containing material with a top coat.

Evidence of silicon oxide etch mask formation from PTMSS oxidation in the first RIE step was provided by cross-sectional TEM, with elemental mapping of oxygen, carbon, and silicon from EELS on the directed PTMSS-*b*-PMOST$_{19.9}$ film stack. A cross section of the sample was imaged after DSA and after removal of the top coat but before etching. A second image and mapping was acquired after a partial O_2 RIE on the same film to study changes in the elemental composition of the film changes upon oxidation. Before etching (Figure 3a), silicon is present only in 10 nm wide rectangular domains within areas that contain only carbon and oxygen. This is expected because silicon should be present only in the PTMSS domain and 10 nm wide structures are consistent with the half-pitch of PTMSS-*b*-PMOST$_{19.9}$. From Figure 3b, it is also apparent that alternating silicon-containing domains penetrate approximately 8 nm deeper into the film than the alternating set. The small gap between the silicon-containing domain and the DLC is interpreted as the PS backfilling brush. One likely interpretation of the observed configuration is that alternating PTMSS domains sit on top of the PS mat stripes composed only of carbon, further supporting the guiding mechanism proposed in Figure 1c and in accordance with the wetting behavior observed during water contact angle measurements. This guiding mechanism has been suggested by other researchers, but to the best of our knowledge, this is the first direct observation.[47] The relative content of silicon, oxygen, and carbon in the horizontal line scan across the domains is also consistent with the expected elemental composition. The silicon and oxygen content in the PTMSS and PMOST domains, respectively, constitute approximately 5−10% of the total composition of each domain, which is consistent (within measurement error) with a 1:11 silicon to carbon and 1:9 oxygen to carbon atomic ratio. Note that the elevated oxygen content in the PTMSS domain is probably overrepresented since the silicon likely oxidizes during the TEM sample preparation.

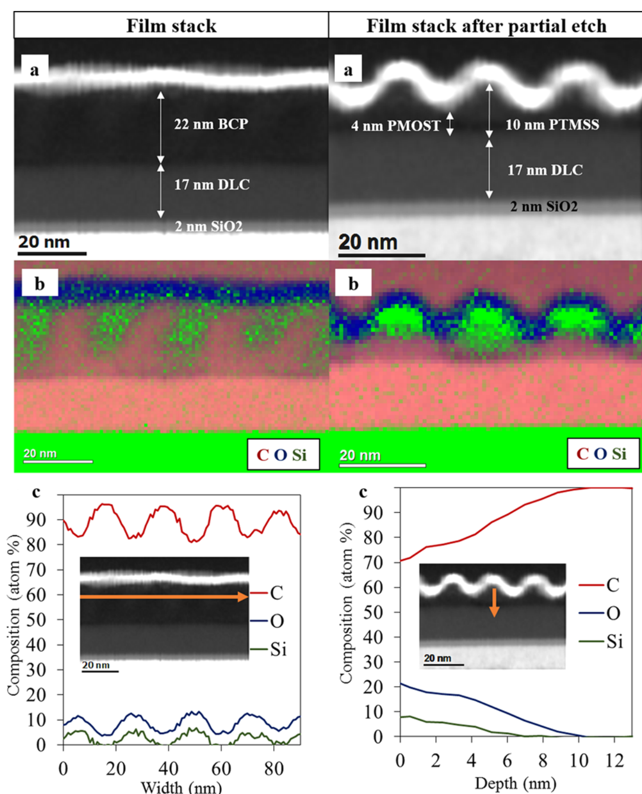

Figure 3. Cross-sectional TEM analysis of a PTMSS-*b*-PMOST$_{19.9}$ film stack aligned by double-patterned sidewall DSA on DLC on silicon with a native oxide layer after annealing and after a partial O_2 RIE. (a) Cross-sectional TEM image with dimensions, (b) EELS mapping of image a showing (red) carbon, (blue) oxygen, and (green) silicon content, and (c) carbon, oxygen, and silicon composition across the arrows indicated in the inset images (reproduced from images in panel a).

After we performed the same oxygen RIE recipe used in the transfer of the pattern in Figure 2c but for a shorter time in order to only partially remove the PMOST, it is again apparent that every other silicon-containing domain sits on top of a material composed only of carbon (likely the mat line; Figure 3b). From the image and analysis of the elemental composition perpendicular to the plane of the film in the silicon domain, it appears that the silicon in the domain densifies and shrinks in the *z*-direction during the O_2 RIE. The domains on top of the mat lines appear to have undergone complete oxidation during this etch based on the homogeneous silicon and oxygen content of the entire domain. In the alternating domains that penetrate further toward the DLC, there appears to be a gradient (partial oxidation) of the silicon consistent with the fact that etching has not been carried out all the way to the DLC. This shows that the PTMSS oxidizes as the domain surface is exposed to the O_2 etch to form ∼3 nm of a silicon oxide etch mask that is apparently sufficient to transfer a pattern into 18 nm DLC. The difference in the total amount of Si between the alternating lines may explain the observed difference in average line width observed on the top-down SEM measurements.

A second observation in Figure 3b is that the domains are tilted. The tilt could be an artifact of sample preparation or could arise from differences in mechanical properties at the interface between the top coat and BCP during annealing. One important change that was implemented during the optimization of the pattern transfer in Figure 2 significantly reduced bridging defects that were initially observed in the pattern transfer. Initially, a low bias was used in the first O_2 RIE step with the rationale that compared to a high bias step, a low bias would make the etch more isotropic and more fully oxidize the sidewalls of the silicon-containing domain. However, bridge defects appeared during this step and propagated to the transferred line pattern shown in Figure 4a. Surprisingly, switching to a higher bias first O_2 RIE step resulted not only in adequate silicon oxidation and pattern transfer, but also in the propagation of significantly fewer bridging defects (Figure 4b). The etch optimization results suggest that the high bias initial step breaks through the thin part of the bridges, leading to the lower defect rates observed in Figure 4b.

■ CONCLUSIONS

In summary, a new double-patterned sidewall directed self-assembly (DSA) was demonstrated with symmetric silicon containing PTMSS-*b*-PMOST block copolymers that were thermally annealed with a top coat. The technique significantly reduces the resolution demands on the guide line lithography. It is well suited for sub-10 nm DSA (sub-20 nm full pitch) because it relaxes the resolution requirements for the resist width from $w_r = {}^1/_2\, L_o$ to $w_r = L_o$. Two lithographically relevant dimensions were demonstrated: 19.9 and 17.4 nm full pitch. The proposed guiding mechanism, which uses chemical contrast from the oxidized sidewalls of cross-linked polystyrene as the guiding interfaces, was supported by a series of experiments probing the wetting behavior of the materials in the guiding pattern and elemental mapping of a cross section of the film stack. The aligned patterns were transferred into a silicon substrate by a series of RIE steps to provide patterns with good sidewall quality and roughness. The oxidation of the silicon in the PTMSS domain during formation of the etch mask was characterized by elemental mapping of a partially oxidized film stack and the defect rate was reduced during this step by optimizing the O_2 etch conditions.

DOI: 10.1021/acsami.5b02481
ACS Appl. Mater. Interfaces 2015, 7, 13476−13483

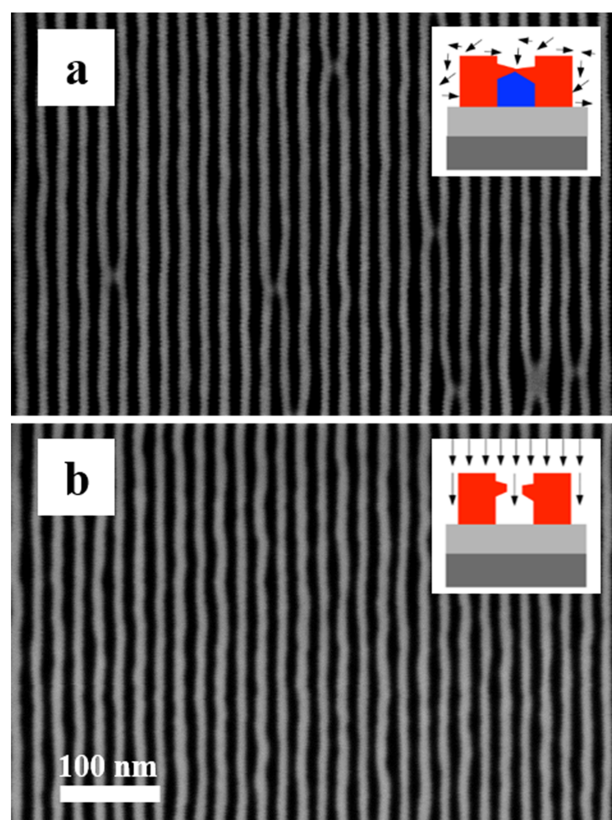

Figure 4. (a) PTMSS-*b*-PMOST$_{19.9}$ lines after pattern transfer using low bias O_2 RIE step (b) PTMSS-*b*-PMOST$_{19.9}$ lines after pattern transfer using high bias O_2 RIE. The insets in each figure suggest the reason for defect reduction in moving to a high bias O_2 etch step.

■ MATERIALS AND METHODS

The guiding lines used in the chemical patterns were written by an Elionix rotary e-beam tool on 50 nm ZEP resist which was coated on 8 nm cross-linked polystyrene mat provided by AZ materials. The mat had been cross-linked by heating to 290 °C for 2 h on top of a 17 nm thick layer of diamond-like carbon that had previously been deposited by ion beam deposition on a silicon substrate. After writing the circumferential line pattern on the resist, developing it, and etching the exposed areas to the DLC with an O_2 RIE, hydroxyl-functionalized polystyrene from Polymer Source with a molecular weight of 1.2 kDa was grafted to the oxidized DLC at 200 °C for 30 min.

PTMSS-*b*-PMOST$_{19.9}$ characterization data can be found in a report that used the same materials[13] and the characterization data for PTMSS-*b*-PMOST$_{17.5}$ are provided in the Supporting Information. The BCP materials were annealed beneath a spin-coatable top coat using a procedure developed previously. Briefly, the BCPs were spin-cast on chemical contrast patterns from 1 wt % solutions in MIBK at various spin speeds to control film thickness. For both fingerprint and DSA patterns, approximately 30 nm thick top coats were spin coated from methanol. PTMSS-*b*-PMOST$_{19.9}$ samples were then annealed at 200 °C for 1.5 min and PTMSS-*b*-PMOST$_{17.4}$ samples were annealed at 180 °C for 4 min on a hot plate in air. These thickness and annealing conditions were optimized to avoid the dewetting and intermixing of the BCP and TC films that was observed under some conditions. Top coats were removed by rinsing the sample with a 5:1 methanol/40% trimethylamine solution in water solution and then subsequently rinsed thoroughly with methanol.

RIE was performed using a PlasmaTherm tool. SEM images were collected on a Zeiss Supra scanning electron microscope. Film thicknesses were measured by scratching films and measuring the height by AFM. AFM images were collected on an ICON AFM. Cross-sectional TEM images with EELS mapping on PTMSS-*b*-PMOST$_{19.9}$ samples were provided by Nanolabs.

■ ASSOCIATED CONTENT

Supporting Information

Characterization data for the materials in this work; water contact angles of the relevant surface materials in this study; AFM trace of the chemical contrast pattern with the backfill brush and corresponding height profile of the guiding line and trench; low-magnification SEM image of terracing with incommensurate film thickness on sidewall-guiding pattern; SEM image of PTMSS-*b*-PMOST when aligned on a guiding pattern with a pitch of 80 nm and a line width of 40 nm; EELS mapping of individual elements in the BCP film stack that corresponds to Figure 3a in the main text; EELS mapping of individual elements in partially etched BCP film stack that corresponds to Figure 3b in the main text. The Supporting Information is available free of charge on the ACS Publications website at DOI: 10.1021/acsami.5b02481.

■ AUTHOR INFORMATION

Corresponding Author

*E-mail: Julia.Cushen@hgst.com.

Author Contributions

The manuscript was written through contributions of all authors. All authors have given approval to the final version of the manuscript.

Notes

The authors declare no competing financial interest.

■ ACKNOWLEDGMENTS

The authors from the University of Texas thank Nissan Chemical Company, the ASTC, and the Rashid Engineering Regents Chair for financial support. The work at UT was also supported in part by the National Science Foundation Scalable Nanomanufacturing Program under Grant No. 1120823 to C.W. G.B. thanks the Paul D. Meek Endowed Graduate Fellowship in Engineering for support. M.M. thanks the IBM Ph.D Fellowship for support. C. Ellison acknowledges partial financial support from the Welch Foundation Grant No. F-1709. Material from UT is based upon work supported by the National Science Foundation Graduate Research Fellowship under Grant No. DGE-1110007 to M.M. Any opinion, findings, and conclusions or recommendations expressed in this material are those of the authors and do not necessarily reflect the views of the National Science Foundation.

■ ABBREVIATIONS

PS-*b*-PMMA polystyrene-*block*-poly(methyl methacrylate)
RIE reactive ion etching
DSA directed self-assembly
BCP block copolymer
PTMSS-*b*-PMOST poly(trimethylsilyl styrene)-*block*-poly-(methoxystyrene)
DLC diamond-like carbon

DOI: 10.1021/acsami.5b02481
ACS Appl. Mater. Interfaces 2015, 7, 13476−13483

REFERENCES

(1) Bates, C. M.; Maher, M. J.; Janes, D. W.; Ellison, C. J.; Willson, C. G. Block Copolymer Lithography. *Macromolecules* **2014**, *47*, 2−12.

(2) Albrecht, T. R.; Bedau, D.; Dobisz, E.; Gao, H.; Grobis, M.; Hellwig, O.; Kercher, D.; Lille, J.; Marinero, E.; Patel, K.; Ruiz, R.; Schabes, M. E.; Wan, L.; Weller, D.; Wu, T. Bit Patterned Media at 1 Tdot/in^2 and Beyond. *IEEE Trans. Magn.* **2013**, *49*, 773−778.

(3) Bencher, C.; Smith, J.; Miao, L.; Cai, C.; Chen, Y.; Cheng, J. Y.; Sanders, D. P.; Tjio, M.; Truong, H. D.; Holmes, S.; Hinsberg, W. D. Self-Assembly Patterning for Sub-15nm Half-Pitch: A Transition From Lab to Fab. *Proc. SPIE* **2011**, *7970*, 79700F.

(4) Tsai, H.; Pitera, J. W.; Miyazoe, H.; Bangsaruntip, S.; Engelmann, S. U.; Liu, C.-C.; Cheng, J. Y.; Bucchignano, J. J.; Klaus, D. P.; Joseph, E. A.; Sanders, D. P.; Colburn, M. E.; Guillorn, M. A. Two-Dimensional Pattern Formation Using Graphoepitaxy of PS-*b*-PMMA Block Copolymers for Advanced FinFET Device and Circuit Fabrication. *ACS Nano* **2014**, *8*, 5227−5232.

(5) Ruiz, R.; Dobisz, E.; Albrecht, T. R. Rectangular Patterns Using Block Copolymer Directed Assembly for High Bit Aspect Ratio Patterned Media. *ACS Nano* **2011**, *5*, 79−84.

(6) Wan, L.; Ruiz, R.; Gao, H.; Patel, K. C.; Lille, J.; Zeltzer, G.; Dobisz, E. A.; Bogdanov, A.; Nealey, P. F.; Albrecht, T. R. Fabrication of Templates with Rectangular Bits on Circular Tracks by Combining Block Copolymer Directed Self-Assembly and Nanoimprint Lithography. *J. Micro/Nanolithogr., MEMS, MOEMS* **2012**, *11*, 031405.

(7) Anastasiadis, S. H.; Russell, T. P.; Satija, S. K.; Majkrzak, C. F. Neutron Reflectivity Studies of the Surface-Induced Ordering of Diblock Copolymer Films. *Phys. Rev. Lett.* **1989**, *62*, 1852−1855.

(8) Chevalier, X.; Nicolet, C.; Tiron, R.; Gharbi, A.; Argoud, M.; Pradelles, J.; Delalande, M.; Cunge, G.; Fleury, G.; Hadziioannou, G.; Navarro, C. Scaling-Down Lithographic Dimensions with Block-Copolymer Materials: 10-nm-Sized Features with Poly(styrene)-*block*-poly(methylmethacrylate). *J. Micro/Nanolithogr., MEMS, MOEMS* **2013**, *12*, 031102.

(9) Zhao, Y.; Sivaniah, E.; Hashimoto, T. SAXS Analysis of the Order−Disorder Transition and the Interaction Parameter of Polystyrene-*block*-poly(methyl methacrylate). *Macromolecules* **2008**, *41*, 9948−9951.

(10) Jung, Y.-S.; Ross, C. A. Orientation-Controlled Self-Assembled Nanolithography Using a Polystyrene-Polydimethylsiloxane Block Copolymer. *Nano Lett.* **2007**, *7*, 2046−2050.

(11) Cushen, J. D.; Otsuka, I.; Bates, C. M.; Halila, S.; Fort, S.; Rochas, C.; Easley, J. A.; Rausch, E. L.; Thio, A.; Borsali, R.; Willson, C. G.; Ellison, C. J. Oligosaccharide/Silicon-Containing Block Copolymers with 5 nm Features for Lithographic Applications. *ACS Nano* **2012**, *6*, 3424−3433.

(12) Cushen, J. D.; Bates, C. M.; Rausch, E. L.; Dean, L. M.; Zhou, S. X.; Willson, C. G.; Ellison, C. J. Thin Film Self-Assembly of Poly(trimethylsilylstyrene-*b*-D,L-lactide) with Sub-10 nm Domains. *Macromolecules* **2012**, *45*, 8722−8728.

(13) Bates, C. M.; Seshimo, T.; Maher, M. J.; Durand, W. J.; Cushen, J. D.; Dean, L. M.; Blachut, G.; Ellison, C. J.; Willson, C. G. Polarity-Switching Top Coats Enable Orientation of Sub-10-Nm Block Copolymer Domains. *Science* **2012**, *338*, 775−779.

(14) Maher, M. J.; Bates, C. M.; Blachut, G.; Sirard, S.; Self, J. L.; Carlson, M. C.; Dean, L. M.; Cushen, J. D.; Durand, W. J.; Hayes, C. O.; Ellison, C. J.; Willson, C. G. Interfacial Design for Block Copolymer Thin Films. *Chem. Mater.* **2014**, *26*, 1471−1479.

(15) Durand, W. J.; Blachut, G.; Maher, M. J.; Sirard, S.; Tein, S.; Carlson, M. C.; Asano, Y.; Zhou, S. X.; Lane, A. P.; Bates, C. M.; Ellison, C. J.; Willson, C. G. Design of High-c Block Copolymers for Lithography. *J. Polym. Sci., Part A: Polym. Chem.* **2015**, *53*, 344−352.

(16) Seshimo, T.; Bates, C. M.; Dean, L. M.; Cushen, J. D.; Durand, W. J.; Maher, M. J.; Ellison, C. J.; Willson, C. G. Block Copolymer Orientation Control Using a Top-Coat Surface Treatment. *J. Photopolym. Sci. Technol.* **2012**, *25*, 125−130.

(17) Cheng, J. Y.; Rettner, C. T.; Sanders, D. P.; Kim, H.-C.; Hinsberg, W. D. Dense Self-Assembly on Sparse Chemical Patterns: Rectifying and Multiplying Lithographic Patterns Using Block Copolymers. *Adv. Mater.* **2008**, *20*, 3155−3158.

(18) Cheng, J. Y.; Sanders, D. P.; Truong, H. D.; Harrer, S.; Friz, A.; Holmes, S.; Colburn, M.; Hinsberg, W. D. Simple and Versatile Methods to Integrate Directed Self-Assembly with Optical Lithography Using a Polarity-Switched Photoresist. *ACS Nano* **2010**, *4*, 4815−4823.

(19) Maher, M. J.; Rettner, C. T.; Bates, C. M.; Blachut, G.; Carlson, M. C.; Durand, W. J.; Ellison, C. J.; Sanders, D. P.; Cheng, J. Y.; Willson, C. G. Directed Self-Assembly of Silicon-Containing Block Copolymer Thin Films. *ACS Appl. Mater. Interfaces* **2015**, *7*, 3323−3328.

(20) Ouk Kim, S.; Solak, H. H.; Stoykovich, M. P.; Ferrier, N. J.; de Pablo, J. J.; Nealey, P. F. Epitaxial Self-Assembly of Block Copolymers on Lithographically Defined Nanopatterned Substrates. *Nature* **2003**, *424*, 411−414.

(21) Delgadillo, P. R.; Gronheid, R.; Thode, C. J.; Wu, H.; Yi, C.; Neisser, M.; Somervell, M.; Nafus, K.; Nealey, P. F. Implementation of a Chemo-Epitaxy Flow for Directed Self-Assembly on 300-mm Wafer Processing Equipment. *J. Micro/Nanolithogr., MEMS, MOEMS* **2012**, *11*, 031302.

(22) Liu, C.-C.; Nealey, P. F.; Raub, A. K.; Hakeem, P. J.; Brueck, S. R. J.; Han, E.; Gopalan, P. Integration of Block Copolymer Directed Assembly with 193 Immersion Lithography. *J. Vac. Sci. Technol., B* **2010**, *28*, C6B30.

(23) Liu, C.-C.; Han, E.; Onses, M. S.; Thode, C. J.; Ji, S.; Gopalan, P.; Nealey, P. F. Fabrication of Lithographically Defined Chemically Patterned Polymer Brushes and Mats. *Macromolecules* **2011**, *44*, 1876−1885.

(24) Han, E.; Stuen, K. O.; La, Y.-H.; Nealey, P. F.; Gopalan, P. Effect of Composition of Substrate-Modifying Random Copolymers on the Orientation of Symmetric and Asymmetric Diblock Copolymer Domains. *Macromolecules* **2008**, *41*, 9090−9097.

(25) Han, E.; Stuen, K. O.; Leolukman, M.; Liu, C.-C.; Nealey, P. F.; Gopalan, P. Perpendicular Orientation of Domains in Cylinder-Forming Block Copolymer Thick Films by Controlled Interfacial Interactions. *Macromolecules* **2009**, *42*, 4896−4901.

(26) Han, E.; Gopalan, P. Cross-Linked Random Copolymer Mats as Ultrathin Nonpreferential Layers for Block Copolymer Self-Assembly. *Langmuir* **2010**, *26*, 1311−1315.

(27) Kim, S.; Bates, C. M.; Thio, A.; Cushen, J. D.; Ellison, C. J.; Willson, C. G.; Bates, F. S. Consequences of Surface Neutralization in Diblock Copolymer Thin Films. *ACS Nano* **2013**, *7*, 9905−9919.

(28) Bates, C. M.; Strahan, J. R.; Santos, L. J.; Mueller, B. K.; Bamgbade, B. O.; Lee, J. A.; Katzenstein, J. M.; Ellison, C. J.; Willson, C. G. Polymeric Cross-Linked Surface Treatments for Controlling Block Copolymer Orientation in Thin Films. *Langmuir* **2011**, *27*, 2000−2006.

(29) Ruiz, R.; Sandstrom, R. L.; Black, C. T. Induced Orientational Order in Symmetric Diblock Copolymer Thin Films. *Adv. Mater.* **2007**, *19*, 587−591.

(30) Dupont-Gillain, C. C.; Adriaensen, Y.; Derclaye, S.; Rouxhet, P. G. Plasma-Oxidized Polystyrene: Wetting Properties and Surface Reconstruction. *Langmuir* **2000**, *16*, 8194−8200.

(31) Cai, C.; Padhi, D.; Seamons, M.; Bencher, C.; Ngai, C.; Kim, B. H. Defect Gallery and Bump Defect Reduction in the Self-Aligned Double Patterning Module. *IEEE Trans. Semicond. Manufact.* **2011**, *24*, 145−150.

(32) Wise, R. Advanced Plasma Etch Technologies for Nanopatterning. *J. Micro/Nanolithogr., MEMS, MOEMS* **2013**, *12*, 041311.

(33) Yaegashi, H.; Oyama, K.; Hara, A.; Natori, S.; Yamauchi, S. Overview: Continuous Evolution on Double-Patterning Process. *Proc. SPIE* **2012**, *8325*, 83250B.

(34) Liu, C.-C.; Ramírez-Hernández, A.; Han, E.; Craig, G. S. W.; Tada, Y.; Yoshida, H.; Kang, H.; Ji, S.; Gopalan, P.; de Pablo, J. J.; Nealey, P. F. Chemical Patterns for Directed Self-Assembly of Lamellae-Forming Block Copolymers with Density Multiplication of Features. *Macromolecules* **2013**, *46*, 1415−1424.

(35) Pickett, G. T.; Witten, T. A.; Nagel, S. R. Equilibrium Surface Orientation of Lamellae. *Macromolecules* **1993**, *26*, 3194−3199.

(36) Kim, H.-C.; Rettner, C. T.; Sundström, L. The Fabrication of 20 nm Half-Pitch Gratings by Corrugation-Directed Self-Assembly. *Nanotechnology* **2008**, *19*, 235301.

DOI: 10.1021/acsami.5b02481
ACS Appl. Mater. Interfaces 2015, 7, 13476−13483

(37) Hong, S. W.; Huh, J.; Gu, X.; Lee, D. H.; Jo, W. H.; Park, S.; Xu, T.; Russell, T. P. Unidirectionally Aligned Line Patterns Driven by Entropic Effects on Faceted Surfaces. *Proc. Natl. Acad. Sci. U.S.A.* **2012**, *109*, 1402−1406.
(38) Hong, S. W.; Voronov, D. L.; Lee, D. H.; Hexemer, A.; Padmore, H. A.; Xu, T.; Russell, T. P. Controlled Orientation of Block Copolymers on Defect-Free Faceted Surfaces. *Adv. Mater. 24*, 4278−4283.
(39) Park, S. M.; Stoykovich, M. P.; Ruiz, R.; Zhang, Y.; Black, C. T.; Nealey, P. F. Directed Assembly of Lamellae- Forming Block Copolymers by Using Chemically and Topographically Patterned Substrates. *Adv. Mater.* **2007**, *19*, 607−611.
(40) Ruiz, R.; Ruiz, N.; Zhang, Y.; Sandstrom, R. L.; Black, C. T. Local Defectivity Control of 2D Self-Assembled Block Copolymer Patterns. *Adv. Mater.* **2007**, *19*, 2157−2162.
(41) Coulon, G.; Russell, T. P.; Deline, V. R.; Green, P. F. Surface-Induced Orientation of Symmetric, Diblock Copolymers: a Secondary Ion Mass-Spectrometry Study. *Macromolecules* **1989**, *22*, 2581−2589.
(42) Peters, R. D.; Yang, X. M.; Kim, T. K.; Sohn, B. H.; Nealey, P. F. Using Self-Assembled Monolayers Exposed to X-Rays to Control the Wetting Behavior of Thin Films of Diblock Copolymers. *Langmuir* **2000**, *16*, 4625−4631.
(43) Walton, D. G.; Kellogg, G. J.; Mayes, A. M.; Lambooy, P.; Russell, T. P. A Free Energy Model for Confined Diblock Copolymers. *Macromolecules* **1994**, *27*, 6225−6228.
(44) Han, E.; Kang, H.; Liu, C.-C.; Nealey, P. F.; Gopalan, P. Graphoepitaxial Assembly of Symmetric Block Copolymers on Weakly Preferential Substrates. *Adv. Mater.* **2010**, *22*, 4325−4329.
(45) Ruiz, R.; Wan, L.; Lille, J.; Patel, K. C.; Dobisz, E.; Johnston, D. E.; Kisslinger, K.; Black, C. T. Image Quality and Pattern Transfer in Directed Self Assembly with Block-Selective Atomic Layer Deposition. *J. Vac. Sci. Technol., B* **2012**, *30*, 06F202.
(46) Albrecht, T. R.; Hellwing, O.; Ruiz, R.; Schabes, M. E.; Terris, B. D.; Wu, X. Z. Bit-Patterned Magnetic Recording: Nanoscale Magnetic Islands for Data Storage. In *Nanoscale Magnetic Materials and Applications*. Liu, J. P.; Fullerton, E.; Gutfleisch, O.; Sellmyer, D. J., Eds; Springer US: Boston, MA, 2009; pp 237−274.
(47) Kim, J.; Wan, J.; Miyazaki, S.; Yin, J.; Cao, Y.; Her, Y. J.; Wu, H.; Shan, J.; Kurosawa, K.; Lin, G. The SMART Process for Directed Block Co-Polymer Self-Assembly. *J. Photopolym. Sci. Technol.* **2013**, *26*, 573−579.

DOI: 10.1021/acsami.5b02481
ACS Appl. Mater. Interfaces 2015, 7, 13476−13483